Since January 2020 Elsevier has created a COVID-19 resource centre with free information in English and Mandarin on the novel coronavirus COVID-19. The COVID-19 resource centre is hosted on Elsevier Connect, the company's public news and information website.

Brain, Behavior, and Immunity 60 (2017) 71–83

Contents lists available at ScienceDirect

Brain, Behavior, and Immunity

journal homepage: www.elsevier.com/locate/ybrbi

Full-length Article

Activated GL7$^+$ B cells are maintained within the inflamed CNS in the absence of follicle formation during viral encephalomyelitis

Krista D. DiSano [a,b], Stephen A. Stohlman [a,1], Cornelia C. Bergmann [a,*]

[a] Department of Neurosciences, Lerner Research Institute, Cleveland Clinic Foundation, 9500 Euclid Avenue, NC30, Cleveland, OH 44195, United States
[b] School of Biomedical Sciences, Kent State University, Kent, OH 44242, United States

ARTICLE INFO

Article history:
Received 10 June 2016
Received in revised form 13 September 2016
Accepted 18 September 2016
Available online 19 September 2016

Keywords:
CNS
Neuroimmunology
B cell
Ectopic follicle
T cell
Viral encephalomyelitis

ABSTRACT

Central nervous system (CNS) inflammation associated with viral infection and autoimmune disease results in the accumulation of B cells in various differentiation stages. However, the contribution between peripheral and CNS activation remains unclear. During gliatropic coronavirus induced encephalomyelitis, accumulation of protective antibody secreting cells is preceded by infiltration of B cells with a naïve and early differentiation phenotype (Phares et al., 2014). Investigation of the temporal dynamics of B cell activation in draining cervical lymph nodes (CLN) and the CNS revealed that peak CNS infiltration of early activated, unswitched IgD$^+$ and IgM$^+$ B cells coincided with polyclonal activation in CLN. By contrast, isotype-switched IgG$^+$ B cells did not accumulate until peripheral germinal center formation. In the CNS, unswitched B cells were confined to the perivascular space and meninges, with only rare B cell clusters, while isotype-switched B cells localized to parenchymal areas. Although ectopic follicle formation was not observed, more differentiated B cell subsets within the CNS expressed the germinal center marker GL7, albeit at lower levels than CLN counterparts. During chronic infection, CNS IgD^{int} and IgD$^-$ B cell subsets further displayed sustained markers of proliferation and CD4 T cell help, which were only transiently expressed in the CLN. A contribution of local CD4 T cell help to sustain B cell activation was supported by occasional B cells adjacent to T cells. The results suggest that accumulation of differentiated B cell subsets within the CNS is largely dictated by peripheral activation, but that local events contribute to their sustained activation independent of ectopic follicle formation.

1. Introduction

Central nervous system (CNS) inflammation as a result of viral infection, tissue injury, or autoimmunity recruits B cell subsets in various differentiation stages ranging from naïve, unswitched and isotype class switched memory B cells (B_{mem}), and antibody secreting cells (ASC) (Ankeny et al., 2009; Cepok et al., 2005; Corcione et al., 2004; Cruz et al., 1987; Dang et al., 2015; Metcalf et al., 2013; Niino et al., 2009; Phares et al., 2014). ASC and their antibody (Ab) specificity have been a major focus in multiple sclerosis (MS) research due to their potential reactivity to autoantigens. Although cerebrospinal fluid (CSF) immunoglobulin (Ig), a diagnostic hallmark, is suggested to be pathogenic, Ig specificity is diverse, rarely targeting myelin antigens (Avasarala et al., 2001; Cruz et al., 1987; Warren and Catz, 1994). Interest in other functions of B cells emerged when clinical trials revealed that the anti-CD20 Ab, Rituximab, which depletes all B cells except ASC, improved clinical symptoms and reduced gadolinium-enhancing lesions in MS patients independent of changes in CSF Ig (Hauser et al., 2008). By contrast, depletion of ASC and mature B cells using TACI Ig (Atacicept) in MS patients increased relapses ultimately resulting in the early termination of clinical trials (Kappos et al., 2014). While the anti-CD20 studies implied a detrimental role for B cells during CNS inflammation apparently independent of Ig secretion, TACI Ig treatment suggested B cells may assume both pathogenic and protective roles during neuroinflammation.

Despite the commonality of distinct B cell subsets in injury, autoimmunity, and viral infection of the CNS, little is known about their activation state, maintenance, or function, especially in relation to peripheral immune activation. In addition to Ig secretion, B cells are important modulators of immune responses during CNS insults. Their functions include antigen presentation, thereby promoting CD4 T cell activities, production of pro- and anti-inflammatory cytokines, and formation of follicle structures, which enhance and maintain local immune responses independent of the periphery (Claes et al., 2015; Michel et al., 2015; Owens et al.,

* Corresponding author.
E-mail address: bergmac@ccf.org (C.C. Bergmann).
[1] Deceased.

http://dx.doi.org/10.1016/j.bbi.2016.09.022
0889-1591/

2011; Pikor et al., 2015). B cells are effective antigen presenting cells and B cell depletion diminishes CD4 T cell numbers, reactivation, and proinflammatory cytokine production in MS patients and in experimental allergic encephalomyelitis (EAE), a rodent model of MS (Parker Harp et al., 2015; Pierson et al., 2014; Weber et al., 2010). B cells can also directly contribute to a proinflammatory milieu within the CNS via production of the cytokines TNF, lymphotoxin (LT), GM-CSF, and IL-6 (Bar-Or et al., 2010; Lehmann-Horn et al., 2011; Lino et al., 2016; Lisak et al., 2012; Malmestrom et al., 2006; Pierson et al., 2014; Xiao et al., 2015). Nevertheless, B cells can also assume anti-inflammatory roles by secreting IL-10 and TGF-β (Lino et al., 2016; Lisak et al., 2012; Tedder, 2015; Xiao et al., 2015). B cell regulation of pathogenic T cells is implicated by exacerbated disease severity coincident with increased CNS encephalitogenic T cells upon B cell depletion prior to EAE induction. Moreover, this regulation was attributed to IL-10 producing B cells (Matsushita et al., 2008, 2010). Subsequent studies further revealed multiple B cell subsets contribute to IL-10 and IL-35 production, including B10 B cells and plasma cells (Maseda et al., 2012; Shen et al., 2014; Tedder, 2015).

Irrespective of defining functions of individual B cell subsets, the broader question of their recruitment and maintenance within the CNS remains under investigation (Claes et al., 2015; Michel et al., 2015; Owens et al., 2011; Pikor et al., 2015). During MS, similar clonality among B cell subsets in the CLN and CNS suggests an axis of continual recruitment after maturation in the periphery (Bankoti et al., 2014; Palanichamy et al., 2014; Stern et al., 2014). However, local factors can further contribute in activating and/or sustaining B cells within the CNS. Lymphoid associated factors that support B cell organization, survival, and differentiation including IL-21, BAFF, CCL19, CCL21, and CXCL13, are all expressed during viral or autoimmune associated CNS inflammation (Kowarik et al., 2012; Krumbholz et al., 2006; Lalor and Segal, 2010; Magliozzi et al., 2004; Metcalf et al., 2013; Phares et al., 2011, 2013a, 2014, 2016; Shi et al., 2001). B cell clusters associated with lymphoid chemokines, dendritic cells, and multiple B cell phenotypes are indeed evident in the CNS during MS and spinal cord injury (SCI) (Ankeny et al., 2006; Magliozzi et al., 2004, 2007; Serafini et al., 2004). Similar structures, often termed ectopic follicles, are also common to chronic infection or autoimmunity at peripheral sites (Bombardieri et al., 2012; Carlsen et al., 2002; Weyand and Goronzy, 2003). While ectopic follicle formation is thus implicated in local B cell survival, activation, and differentiation independent of secondary lymphoid tissue, they are less organized than follicles in lymphoid organs. This questions the extent to which follicle formation is essential for B cell activation and isotype switching. Studies using mice deficient in CXCL13 or its receptor CXCR5, suggest isotype-switched Ab production can occur in the absence of defined follicles and germinal center (GC) formation following both peripheral and CNS infection (Junt et al., 2005; Phares et al., 2016; Rainey-Barger et al., 2011). B cell activation and maturation within the CNS may therefore occur independent of defined follicular structures under suitable conditions, which remain to be defined.

Using neurotropic coronavirus infection, this study aimed to better characterize kinetics, activation and structural organization of B cell subsets in the CNS relative to the cervical lymph nodes (CLN), the primary site for T and B cell activation. In this viral encephalomyelitis model, T cells clear infectious virus within 14 days post infection (p.i.), while ASC emerging within the CNS after initial viral control maintain persisting viral RNA at low levels and prevent recrudescence (Lin et al., 1999; Marques et al., 2011). Isotype-unswitched IgD^+IgM^+, $IgD^{int}IgM^+$, and IgD^-IgM^+ B cells accumulate early during infection prior to ASC and are progressively replaced by more differentiated IgD^-IgM^- class-switched B_{mem} and ASC (Phares et al., 2014). Using flow cytometry and histology we herein show that IgD^+ B cells were recruited to the CNS coincident with activation in CLN prior to GC formation. By contrast, class-switched B cells emerged concurrent with defined GC structures in the CLN, with no evidence for ectopic follicle formation in the CNS. Nevertheless, local CD4 T cell help was supported by sustained expression of proliferation and activation markers by the vast majority of more differentiated IgD^{int} and IgD^- B cells in the CNS as well as occasional CD4 T cell-B cell interactions. Overall, the results suggest initial CNS B cell recruitment is driven by activation events in CLN; however prolonged expression of activation markers on more differentiated B cells in the CNS relative to the CLN support local factors contribute to ongoing activation independent of ectopic follicle formation.

2. Materials and methods

2.1. Mice and infection

Wild type (WT) C57BL/6 mice were purchased from the National Cancer Institute (Frederick, MD). All mice were housed under pathogen free conditions at an accredited facility at the Cleveland Clinic Lerner Research Institute. Six-to seven-week old mice were infected intracranially (i.c.) with 1000 plaque forming units (PFU) of J.2.2v-1 monoclonal Ab variant JHMV (Fleming et al., 1986). All procedures were conducted in accordance with protocols approved by the Institutional Animal Care and Use Committee.

2.2. Cell isolation

For phenotypic analysis, brain or CLN derived mononuclear cells were isolated from pooled organs of 3–6 mice per time point. Briefly, brains were minced and digested in 5 ml RPMI supplemented with 10% fetal calf serum (FCS), 100 μl of collagenase type I (100 mg/ml; Worthington Biochemical Corporation, Lakewood, NJ) and 50 μl of DNase I (100 mg/ml) (Roche, Indianapolis, IN) for 40 min at 37 °C. Collagenase and DNase I activity was terminated by addition of 0.1 M EDTA (pH 7.2) at 37 °C for 5 min. Cell pellets were resuspended in RPMI medium, adjusted to 30% Percoll (Pharmacia, Piscataway, NJ), and underlaid with 1 ml of 70% Percoll. Following centrifugation for 30 min at 850 x g, cells were recovered from the 30/70% Percoll interface, washed with RPMI supplemented with 2% FCS and resuspended in fluorescence-activated cell sorter (FACS) buffer (PBS with 0.5% bovine serum albumin) for flow cytometry or RPMI 1640 supplemented with 2 mM L-Glutamine, 2 mM non-essential amino acids, 1 mM sodium pyruvate, 25 μg/ml gentamicin, 5×10^{-5} M 2-mercaptoethanol, and 10% FCS (RPMI complete) for cell culture. CLN cells were isolated as previously described (Lin et al., 1999).

For feeder layers, spleens from naïve C57BL/6 mice were dissociated mechanically and red blood cells lysed. Resuspended splenocytes were irradiated with 3000 rad using a Shepherd irradiator (JL Shepherd and Associates, San Fernando, CA), washed, resuspended in RPMI complete and $5x10^5$ cells in 0.1 ml plated per well prior to *in vitro* stimulation.

2.3. In vitro B cell stimulation and ELISPOT assay

Brain derived single cell suspensions were resuspended at a starting concentration of $2x10^4$ cells/0.1 ml of RPMI complete containing 0.6 μg/ml LPS or 1 μg/ml multimeric CD40L (Adipogen, San Diego, CA) with 1 ng/ml recombinant mouse IL-4 (BioLegend, San Diego, CA). Cells were plated at 1:2 serial dilutions and stimulated for 3 or 4 (LPS) and 4 or 5 days (CD40L) with irradiated splenocytes. Stimulated cells were washed using prewarmed (37 °C)

RPMI complete three times at 190 g × 5 min, resuspended in RPMI complete and transferred to ELISPOT plates. Total and JHMV-specific IgG ASC were detected by ELISPOT assay as previously described (Phares et al., 2016). Briefly, 96-well MultiScreen HTS IP plates (EMD Millipore, Billerica, MA) were stripped with 50 μl of ice cold 70% ethanol for 2 min and washed three times with 0.1 M Sodium Bicarbonate buffer prior to coating. Plates were coated with either virus (~5×10^5 PFU/well) or polyclonal goat anti-mouse Ig (10 μg/ml; Cappel Laboratories, Inc., Cochranville, PA) overnight at 4°C. Following washing once with 0.05% Tween in PBS (wash buffer) and three times with PBS, binding sites were blocked by incubating plates with RPMI 1640 with 5% FCS for 2 h at 37 °C. Blocking media was replaced by serial dilutions of stimulated cells in RPMI 1640 with 10% FCS plated in triplicate. Following 4 h incubation at 37 °C, plates were washed twice with PBS and twice with wash buffer. ASC were detected by incubation with biotinylated rabbit anti-mouse IgG (0.5 μg/ml; Southern Biotech, Birmingham, AL) overnight at 4 °C. Following four washes in wash buffer, plates were incubated with streptavidin horseradish peroxidase (1:1000; BD biosciences, St. Louis, MO) for 1 h at room temperature, washed twice with wash buffer and twice with PBS. Spots were developed using filtered 3,3′-diaminobenzidine substrate (Sigma–Aldrich, St. Louis, MO) with 0.3% hydrogen peroxide. The reaction was terminated using cold tap water once spots were visible after 2–4 min. Spots were counted using an ImmunoSpot ELISPOT reader (Cellular Technology Ltd., Shaker Heights, OH).

2.4. Flow cytometric analysis

Cells were incubated in FACS buffer supplemented with 1% mixed serum (mouse, goat and horse, 1:1:1) and 0.5 μl per 10^6 cells rat anti-mouse FcγIII/II mAb (2.4G2; BD Bioscience, San Jose, CA) for 20 min on ice prior to staining. Cells were incubated with Fixable viability stain 780 APC-Cy7 (BD Biosciences, San Jose, CA) for 15 min on ice and washed in FACS buffer. Expression of cell surface markers was determined by staining with Ab specific for CD45 (30-F11; PerCP-Cy5.5), CD19 (1D3; PE-CF594), CD80 (16-10A1; PE), CD40 (3/23; PE), GL7 (FITC), CD95 (PE) (BD Biosciences, San Jose, CA), IgM (eB131-15F9; PE), IgD (11-26; APC), and CD38 (90; PE) (eBioscience, San Diego, CA). Plasmacytoid dendritic cells (pDCs) were assessed using anti B220 (RA3-6B2; PE) CD11c (HL3; FITC), PDAC-1 (APC), and CD3 (145-2C11; PE-Cy7) mAbs (BD Biosciences, San Jose, CA). Intracellular staining for Ki-67 (D56; FITC) or IgG isotype control (MOPC-21; FITC) (BD Biosciences, San Jose, CA) was performed after permeabilization with Foxp3 intracellular staining kit (eBioscience). Cells were analyzed on a BD LSRII flow cytometer (BD Biosciences, San Jose, CA) using FlowJo (version 9.7.6) software (Tree Star, Ashland, OR). Cell numbers were calculated based on live cell yields and percentages of gated live cells. Overall gating strategy of B cells is depicted in Supplementary Fig. 1. Dead cells comprised less than 10% and doublets were excluded based on FSC-Area and FSC-Height. Fluorescence minus one (FMO) is shown as a control for GL7 staining. For all results density plots are representative of 3–4 independent experiments.

2.5. Immunohistochemistry

CLN or brains from PBS-perfused mice were snap-frozen in Tissue-Tek OCT compound (Sakura Finetex, Torrance, CA) and sectioned at 10 μm using a Thermo Shandon cryostat. Sections were fixed with either ice cold 70% acetone for 5 min (CLN) or 4% paraformaldehyde (PFA) for 15 min (brain). All washes for brain sections were performed in 0.1% Triton in PBS and for CLN, sections were washed in PBS. Sections were blocked with 5% bovine serum albumin and 10% goat serum for 1 h. After blocking CLN sections were incubated with rat IgM anti mouse FITC conjugated GL7 mAb, rat IgG anti-mouse B220 mAb (BD biosciences, San Jose, CA) and rabbit IgG anti-mouse CD3 polyclonal Ab (Abcam, Cambridge, MA). Primary Abs were detected using secondary Alexa Fluor 594 goat anti-rat and Cy5 goat anti-rabbit Ab (Life Technologies, Grand Island, NY). Brain sections were stained with B220, CD3, donkey anti-mouse IgM (Jackson Immunoresearch), rat anti-mouse IgD (eBioscience, San Diego, CA), rabbit anti-mouse Laminin (Cedarlane, Burlington, NC), rabbit anti-mouse Caspase-3, or rabbit anti-mouse Ki-67 (Abcam, Cambridge, MA), IgG conjugated with Alexa Fluor-594 (Jackson Laboratories, Sacramento CA) followed by addition of secondary Abs Alexa Fluor goat anti-rabbit 488 and Alexa Fluor 594 goat anti-rat or Alexa Fluor goat anti-donkey 594 (Life Technologies, Grand Island, NY). All incubations with primary Ab were overnight at 4 °C and with secondary Ab 1 h at room temperature. Sections were mounted with ProLong Gold antifade reagent with 4′,6-diamidino-2-phenylindole (DAPI) (Life Technologies, Grand Island, NY) and examined using a SP5 Leica confocal microscope or Leica TCS SP5 II multiphoton microscope (Leica Microsystems, Exton, PA) for brain sections. Z-series images were collected at 0.5 um intervals, covering a tissue depth of 8–10 um. Projected images, orthogonal views and 3D views were generated using Image J software (NIH, http://rsbweb.nih.gov/ij) implementing the FIJI plugin set (http://pacific.mpi-cbg.de/wiki/index.php/Fiji). The relative percentage of IgG^+ or IgM^+ cells localizing within the parenchyma or perivascular/meningeal space was calculated using 6–8 Z stack compilations (at power x40; field size = 0.369 mm^2) per time point from 2 to 3 animals. Images were assembled for publication using Adobe Photoshop 7.0 software (Adobe Systems, San Jose CA).

2.6. Statistical analysis

Data were analyzed using Prism (version 6.0) software (GraphPad). Statistical analysis between the experimental groups was assessed using a two-tailed paired *t* test. In all cases, a *P* value of <0.05 was considered significant.

3. Results

3.1. Isotype-switched B cells accumulate in the CNS coincident with robust GC formation within the periphery

The dynamics and temporal relationship of B cell subsets in the CNS relative to CLN, the site of primary lymphocyte activation following CNS infection (Laman and Weller, 2013) is unclear. We therefore initially compared alterations in B cell populations in the CNS and CLN throughout the acute and resolving phase of gliatropic coronavirus infection by flow cytometry (Fig. 1). During acute CNS infection at day 7, the majority of B cells in the CNS displayed a naïve IgD^+IgM^+ (~60%) or activated $IgD^{int}IgM^+$ (22%) phenotype. As the infection resolved the proportion of IgD^-IgM^+ cells stayed constant, while more differentiated IgD^-IgM^- B cells, comprising both isotype-switched B_{mem} and ASC, progressively increased (Fig. 1). By day 21 p.i., over 50% of B cells in the CNS were isotype-switched ASC and B_{mem}, consistent with previous results (Phares et al., 2014). To assess how the progressive accumulation of isotype-switched B cells correlates with differentiation in the periphery, the same phenotypes were monitored in the CLN (Fig. 1). Naïve IgD^+IgM^+ cells comprised the vast majority of $CD19^+$ B cells throughout infection (Fig. 1, >70%), consistent with a small proportion of B cells being activated in the CLN. Although the fraction of activated $IgD^{int}IgM^+$ and IgD^-IgM^+ B cells transiently increased at day 7 p.i., the proportion of isotype-switched IgD^-IgM^- B cells did not significantly increase until day 21 p.i. The elevated proportion of isotype-switched B cells in the CNS

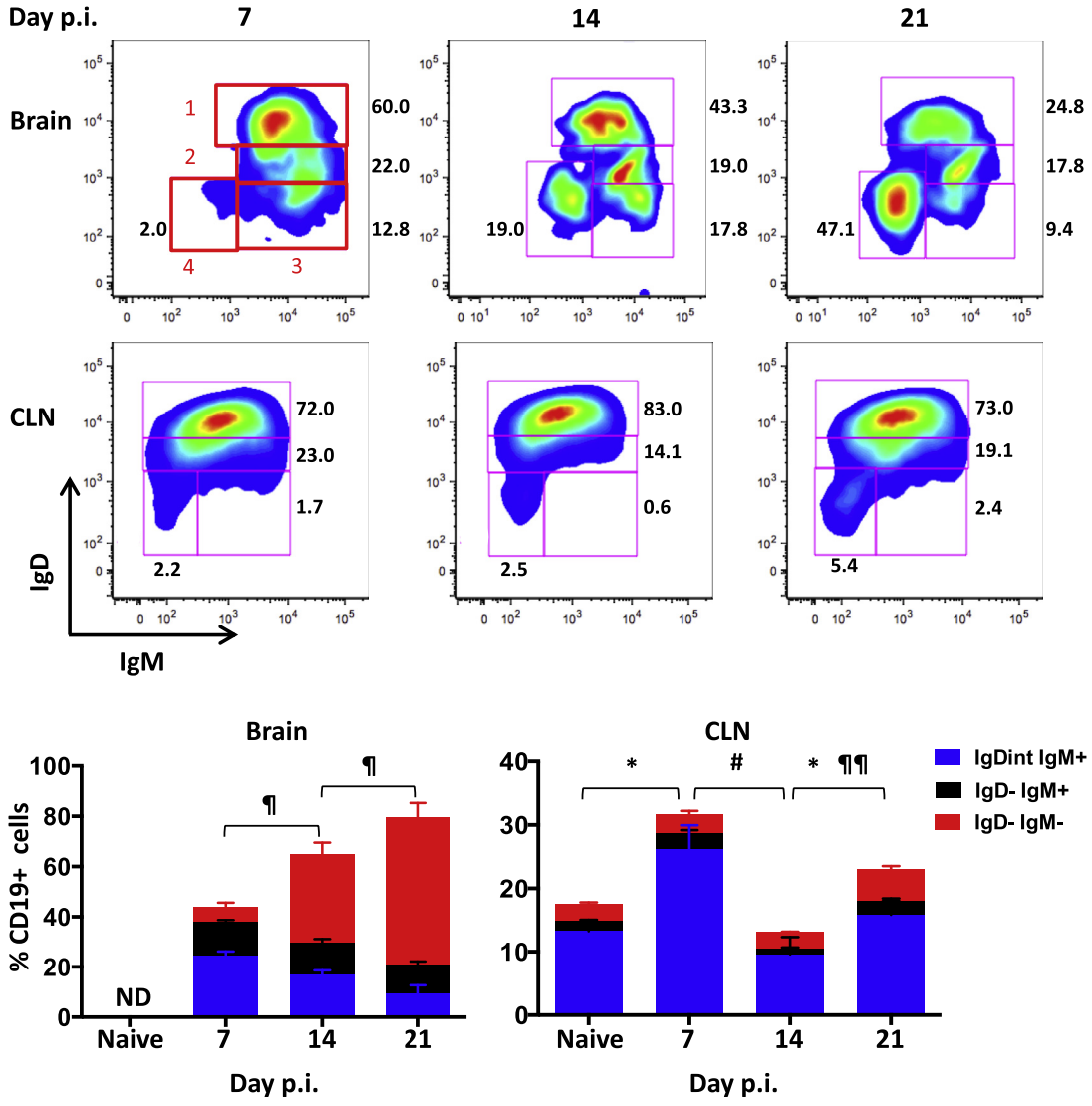

Fig. 1. Dynamics of B cell subsets within the CNS and CLN during JHMV infection. Brain and CLN derived cells isolated from pooled organs of naïve or infected mice at day 7, 14, and 21 p.i. were analyzed for their IgD, IgM, and isotype-switched phenotype by flow cytometry. Representative density plots depict gating strategy for $IgD^{+}IgM^{+}$ naïve B cells (1), $IgD^{int}IgM^{+}$ early activated (2), $IgD^{-}IgM^{+}$ activated (3), and $IgD^{-}IgM^{-}$ isotype-switched (4) within $CD45^{hi}CD19^{+}$ cells from brain and CLN as indicated. Red numbers indicate respective gates and black numbers show percent of populations. Stacked bar graphs show percentages of $IgD^{int}IgM^{+}$, $IgD^{-}IgM^{+}$, and $IgD^{-}IgM^{-}$ cells within $CD45^{hi}CD19^{+}$ cells and their changing dynamics over time. $IgD^{+}IgM^{+}$ naïve B cells make up the remaining percentage of cells. B cells within brains of naïve mice were not detectable (ND). Data are expressed as the mean percentage ± SEM from 3 to 4 independent experiments each comprising 3–6 pooled brain or CLN per time point. Significant differences demarcated by $*$ for IgD^{int} IgM^{+}, # for IgD^{-} IgM^{+}, and ¶ for $IgD^{-}IgM^{-}$ B cell populations with $*$ # ¶ denoting ($p < 0.05$) and ¶¶ denoting ($p < 0.01$). (For interpretation of the references to color in this figure legend, the reader is referred to the web version of this article.)

already evident at day 14 p.i. thus did not reflect dynamics in the periphery. To account for an overall transient increase in CLN cellularity from $\sim 2.5 \times 10^6$ in naïve mice to $\sim 18 \times 10^6$ at day 7 p.i., percentages of B cell subsets were converted to absolute numbers (Fig. 2). A pronounced increase in $CD19^{+}$ B cells in the CLN relative to uninfected mice at day 7 p.i. reflected elevated total cells and coincided with peak B cell infiltration into the brain (Fig. 2). $IgD^{int}IgM^{+}$, $IgD^{-}IgM^{+}$, and isotype-switched B cells also all peaked at day 7 p.i. within the CLN and declined by ~ 70% by day 14 p.i. (Fig. 2A). However, while the less differentiated subsets remained low, isotype-switched B cells increased again moderately by day 21 p.i. In the CNS, IgD^{int} and $IgD^{-}IgM^{+}$ B cell numbers also peaked at day 7 p.i but remained elevated above background thereafter (Fig. 2B). In contrast to their peripheral increase, isotype-switched B cells were barely detectable by day 7 p.i. and only became prominent by day 14 p.i. Overall, the number of B cells in each population in the CNS were at least 100 fold reduced compared to the CLN.

Ectopic follicle formation has been postulated to contribute to ongoing B cell responses remote from peripheral events (Bombardieri et al., 2012; Carlsen et al., 2002; Magliozzi et al., 2007; Serafini et al., 2004; Weyand and Goronzy, 2003). Other studies of chronic inflammation, including MS, provide evidence for an active axis between the CLN and CNS, which maintains CNS populations by continual recruitment of B cells from the periphery (Bankoti et al., 2014; Palanichamy et al., 2014; Stern et al., 2014). We therefore assessed how CLN B cell differentiation correlates with GC formation by immunohistochemistry using GL7 expression as a hallmark of GC B cells (Cervenak et al., 2001; Naito et al., 2007). Of note, GL7 is not only an epitope upregulated on GC B cells, but is also present, albeit at lower levels, on highly activated B cell subsets readying to enter a GC reaction (Balogh

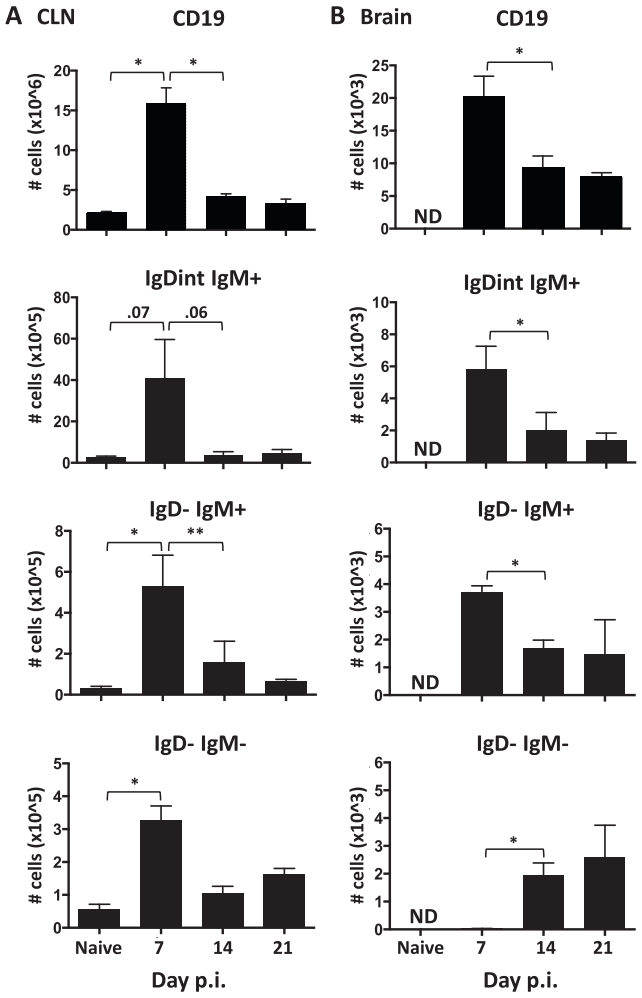

Fig. 2. B cell accumulation within the brain peaks by day 7 p.i. Numbers of total CD19$^+$, IgD^{int}IgM$^+$, IgD$^-$IgM$^+$, and IgD$^-$IgM$^-$ B cells determined by flow cytometry within the CLN (A) and brain (B) in naïve and infected mice at day 7, 14, and 21 p.i. Data are expressed as the mean number ± SEM and represent 3–4 independent experiments each comprising 3–6 pooled brains or CLNs per time point. B cells within brains of naïve mice were not detectable (ND). Significant differences between time points are denoted by ∗ ($p < 0.05$) and ∗∗ ($p < 0.01$).

et al., 2010; Cervenak et al., 2001). CLN in naïve mice showed distinct B cell follicles and T cell zones but were void of GL7$^+$ cells. Weak GL7 reactivity within B cell follicles was detectable at day 7 p.i., suggesting initiation of GC formation (Fig. 3A). By day 14 p.i., GL7$^+$ cells formed well-demarcated structures typical of GCs, but were also loosely scattered within follicles as well as at the T cell/ B cell border. Mature GCs, characterized by distinct light and dark zones, were not evident until day 21 p.i., when infectious virus has already been cleared from the CNS (Phares et al., 2016; Stohlman et al., 1995). GL7 expression was also monitored by flow cytometry to quantify the relative expression as well as the proportion of GC phenotype B cells over time. GL7$^+$ cells comprised a minor population of ~2% within total B cells at day 7 p.i., which increased to ~5% at day 14 p.i. and remained stable throughout day 21 p.i. (Fig. 3B/C). Segregation of GL7$^+$ CD19$^+$ cells into GL7^{hi} and GL7^{int} phenotypes to distinguish GC from activated B cells not participating in GC, revealed that the GL7^{hi} GC proportion increased to ~50% throughout days 14–21 p.i., coincident with bright reactivity and detection of GC by immunohistology. Characterization of the CLN B cell subsets which most prominently upregulated GL7 at day 14 p.i. revealed that the vast majority of GL7^{hi} cells were IgD$^-$ B cells (Fig. 3D and E). Accumulation of isotype-switched B cells in the CNS thus correlated with robust GC formation in CLN at day 14 p.i. By contrast, the earlier peak of isotype-unswitched B cells in the CNS coincided with early B cell activation indicated by IgD downregulation and modest GL7 expression.

The transient early increase of activated IgD^{int} and IgD$^-$ B cells in the CLN is consistent with nonspecific polyclonal activation evident in peripheral viral infection models (Rothaeusler and Baumgarth, 2010). To investigate whether the IgD$^+$ or IgM$^+$ B cells within the CNS are bystander cells or are virus specific, CNS cells were polyclonally activated using LPS/IL-4 or biologically more relevant CD40/IL-4 stimulation and tested for differentiation into virus specific IgG secreting ASC (Hawkins et al., 2013). As a positive control, we initially tested conversion of B cells isolated from the brain at day 7 p.i., which mainly constitute IgD$^+$ cells, into IgG secreting ASC (Supplementary Fig. 2). LPS stimulation for 3 days yielded few IgG secreting ASC, consistent with the minimal requirement of LPS stimulation for 72–96 h to sufficiently convert naïve B cells to ASC (Hawkins et al., 2013). However, after 4 days stimulation IgG secreting ASC were abundant using either LPS or CD40L and IL-4 stimulation. By contrast, assessment of virus specific IgG ASC did not reveal any spot formation at day 7 p.i. Nevertheless, similar analysis of CNS cells isolated at day 21 p.i., when IgD$^-$ B cells prevail, showed elevated numbers of virus specific ASC relative to unstimulated cells. These results suggest that early IgD$^+$ B cells are not virus specific or have too low affinity to be detected by ELISPOT, whereas IgD$^-$ B cells comprise virus specific ASC and memory B cells which can be converted into ASC.

3.2. B cell subsets in the CNS localize to blood vessels and meninges, but do not form ectopic follicles

The data above indicated that early peripheral B cell activation and subsequent GC formation largely drive the sequential emergence of distinct B cell subsets in the CNS. To evaluate an additional contribution of local CNS support in promoting differentiated B cell accumulation, we assessed potential ectopic follicle formation. Analysis of B220$^+$ cell distribution relative to laminin, demarcating the vascular or meningeal basement membrane, revealed predominant localization within the perivascular space and meninges during acute inflammation at day 7 p.i. (Fig. 4A). Although the vast majority of B cells remained at these sites at day 14 p.i., localization of isolated B cells in the parenchyma was indicated by B220$^+$ cells distal to the meninges/vasculature (Fig. 4A, white arrows). By day 21 p.i., parenchymal B cell infiltration was robust (Fig. 4A). The exclusive early localization of B220$^+$ cells to the perivascular space and meninges combined with flow cytometry data suggested they are predominately isotype-unswitched. Furthermore, flow cytometric analysis to verify that B220$^+$ cells were not pDCs revealed that less than 2% had a B220$^+$CD11c$^+$PDAC-1$^+$ CD3$^-$ pDC phenotype (data not shown). Analysis of either IgD$^+$ or IgM$^+$ cells at day 14 p.i. confirmed perivascular and meningeal B cell localization (Fig. 4B and C). Co-labeling with anti-IgD and IgM Abs to examine potentially distinct distribution of IgD$^+$IgM$^+$ or IgD$^-$IgM$^+$ cells showed both phenotypes localized within occasional B cell clusters (Fig. 4D). IgD$^+$ or IgM$^+$ B cells were predominately confined to the perivascular or meningeal space throughout infection (<10%; IgM: Fig. 4F; IgD: data not shown). By contrast, IgG$^+$ cells preferentially localized to the parenchyma with time (Fig. 4E and F), supporting that parenchymal B cells are largely isotype-switched B_{mem} or ASC.

Despite the overall paucity of B cell clusters within the CNS during JHMV infection, occasional clusters in the subpial meninges suggested an environment akin to GC-like follicles may occur. To examine whether B cell clusters revealed hallmarks of defined follicles or GC-like structures, we investigated the presence of follicular dendritic cells, GL7^{hi} cells, proliferation, and apoptosis. We

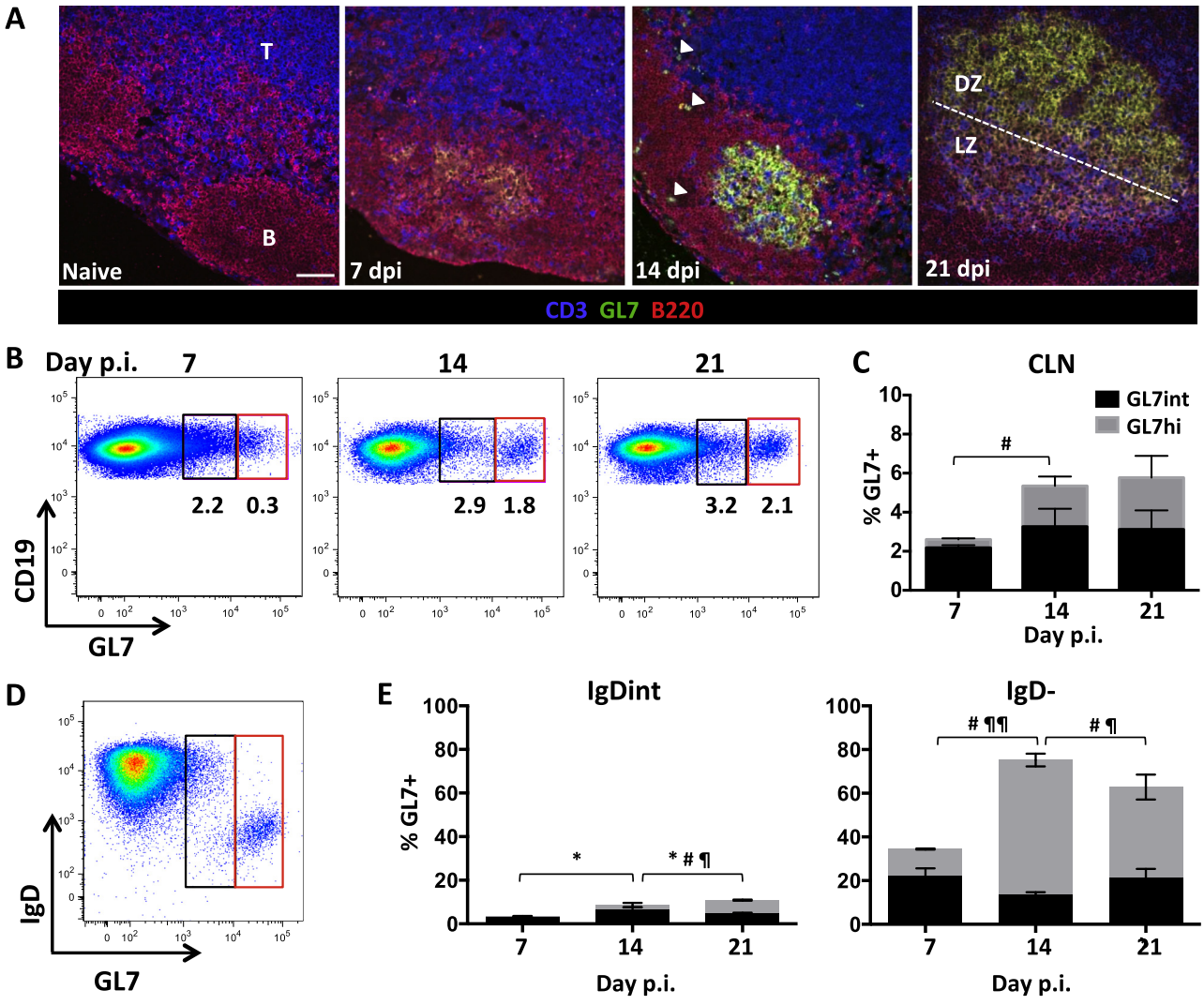

Fig. 3. GC formation is robust within the draining CLN by day 21 p.i. (A) GC formation within CLN of naïve and infected mice at days 7, 14, and 21 p.i. was assessed by immunohistochemistry using *anti*-B220 (red), GL7 (green) to mark GC B cells, and CD3 (blue) mAb. B cell follicles and T cell zones are indicated by (B) and (T) respectively. $GL7^+$ B cells form prominent structures by day 14 p.i.; white arrows indicate occasional $GL7^+$ cells dispersed in follicular areas and the B-T cell border. Light (LZ) and dark zones (DZ) are established at day 21 p.i. Representative images from 2 independent experiments with 3–4 mice per experiment. Scale bar = 50 μm. (B) Representative flow cytometry plots showing GL7 expression by CLN derived $CD19^+$ B cells at day 7, 14, and 21 p.i. $GL7^+$ cells segregate into $GL7^{int}$ (black) activated pre-GC cells and GL7hi (red) B cells typical of GC B cells. (C) Percentages of $GL7^{int}$ (black) and $GL7^{hi}$ (gray) cell within total $CD19^+$ B cells in CLN at day 7,14, and 21 p.i. (D) Representative density plot gated on CLN $CD19^+$ B cells at day 14 p.i. demarcating IgD expression among $GL7^{int}$ and $GL7^{hi}$ populations. (E) Relative percentages of $GL7^{int}$ and $GL7^{hi}$ cells within IgD^+, IgD^{int}, or IgD^- CLN derived $CD19^+$ B cells at day 7, 14, and 21 p.i. Data in (B) and (D) are expressed as the mean percentage ± SEM and represent 3–4 independent experiments each comprising pooled CLN from 3 to 6 mice per time point. Significant differences between time points are indicated by ∗ ($p \leqslant 0.05$) for GL7int, # ($p \leqslant 0.05$) for GL7hi, and ¶ ($p \leqslant 0.05$) or ¶¶ ($p \leqslant 0.01$) for total GL7 + cells. (For interpretation of the references to color in this figure legend, the reader is referred to the web version of this article.)

found no evidence for $CD21/35^+$ follicular dendritic cells or GL7 reactivity (data not shown). Similarly, immunohistochemistry did not reveal prominent B cell expansion using Ki-67 as a nuclear marker of cells in the active phase of cell cycle. While a few individual proliferating B cells were present in the meninges at days 14 and 21 p.i., we could not detect $Ki\text{-}67^+$ B cells in clusters typical of GC. Nevertheless, numerous other Ki-67+ cells were evident in proximity to each other as well as in scattered locations distal to cell clusters (Fig. 5A). Occasionally a proliferating B cell was also observed in close proximity to non B cell lineage $Ki\text{-}67^+$ cells, which were mainly identified as $CD3^+$ T cells (data not shown). In addition to the paucity of clustered proliferating B cells, the absence of GC-like activity was also supported by only a few apoptotic B cells marked by caspase-3 staining (Fig. 5B).

The proportion of proliferating B cells and their phenotype within the CNS over time was evaluated by flow cytometry (Fig. 5 C and D). Proliferation of B cells was minimal at day 7 p.i. (<20%), when they reach peak numbers composed of largely undifferentiated subsets (Fig. 2B). Proliferation rates increased to ~40% by day 14 p.i. and were further elevated to ~75% by day 21 p.i. These kinetics correlated directly with increased accumulation of more differentiated IgD^- B cells by day 21 p.i. (Fig. 1). Indeed, proliferation was most extensive and stable on IgD^-IgM^+ and IgD^-IgM^- populations throughout infection (Fig. 5D). Contrasting these results in the CNS, Ki-67 within the CLN was significantly increased on B cells by day 7 p.i. relative to naive mice, and declined by day 14 p.i. (Fig. 5E). Proliferation was most prominently induced in IgD^-IgM^+ cells at day 7 through day 21 p.i., reaching ~60%. Isotype-switched B cells proliferated at a high rate under steady state conditions in naïve mice (Fig. 5E). Although infection elevated proliferation to 80% by day 14 p.i., percentages of proliferating cells declined to background levels by day 21 p.i.

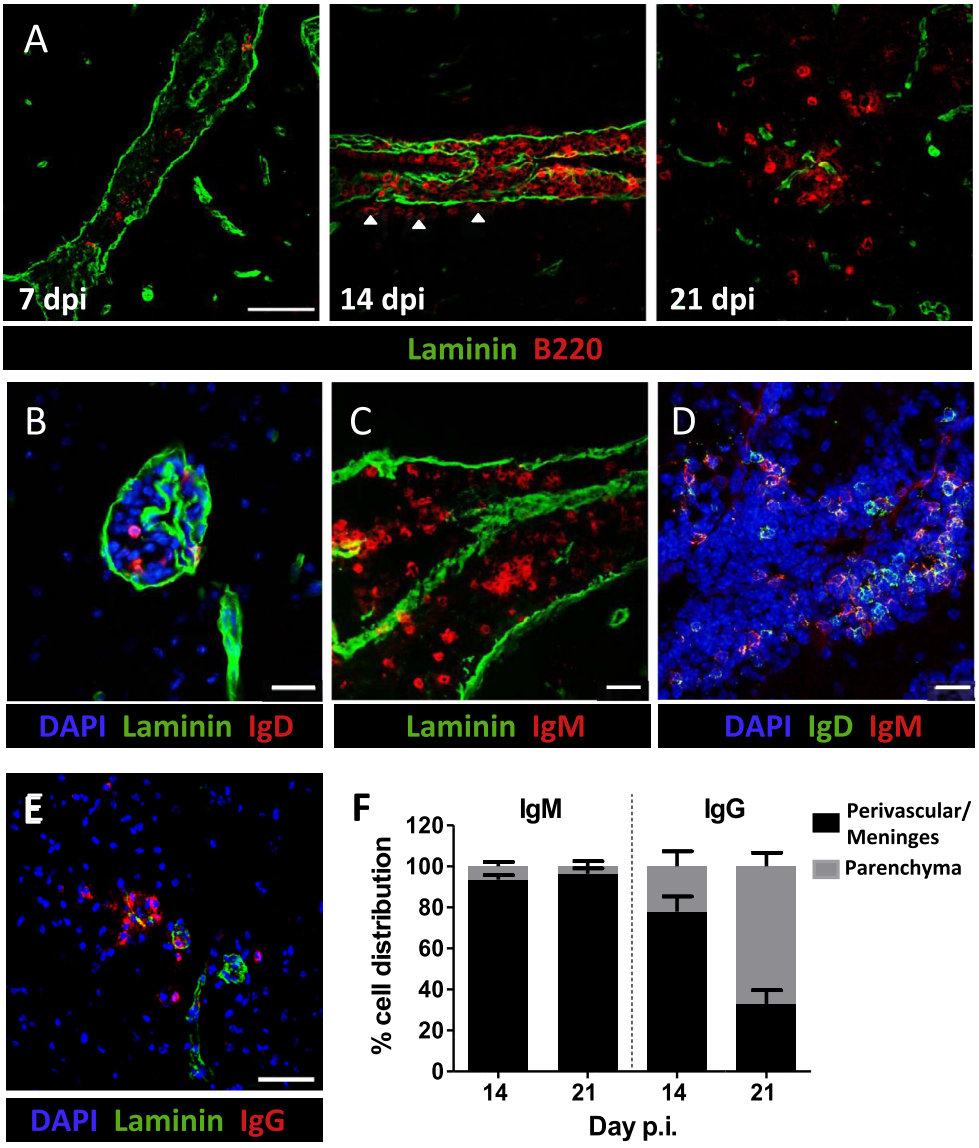

Fig. 4. IgM$^+$ and IgD$^+$ B cells are localized within the meninges and perivascular space. Sagittal brain sections were stained with the indicated combinations of anti-B220, IgD, IgM, IgG, and laminin mAb to identify B cell localization to meninges and blood vessels and relative to basement membranes at day 7,14, and 21 p.i. (dpi) (A) B220$^+$ (red) B cell localization relative to laminin$^+$ (green) structures. Arrows indicate isolated B cells emerging at parenchymal sites at day 14 p.i. (B) IgD$^+$ (red) B cells confined to the perivascular space. (C) IgM$^+$ (red) cells present within the laminin$^+$ subpial meningeal space. (D) Localization of both IgD$^+$IgM$^+$ and IgM$^+$IgD$^-$ B cells within the CNS at d14 p.i. (E) IgG$^+$ (red) B cells and laminin (green) at day 21 p.i. within the CNS. Representative images shown are z stack projected compilations from 2 independent experiments with 3 mice per experiment. (F) Percent distribution of isotype-unswitched (IgM$^+$) and isotype-switched (IgG+) B cells at day 14 and 21 p.i. For quantification, 6–8 Z stacks representing 2–3 animals per time point were counted manually for IgM$^+$ or IgG$^+$ B cells within the parenchyma or perivascular/meningeal space, defined by laminin staining. Data are expressed as the mean percentage ± SEM. Scale bars = 50 μm (A, E) and 20 μm (B–D). (For interpretation of the references to color in this figure legend, the reader is referred to the web version of this article.)

Overall, these results demonstrate that a large and stable proportion of IgD$^-$ B cells within the CNS express Ki-67 independent of local follicle formation. The apparent discrepancy to sparse numbers of Ki-67$^+$ B cells detected by histology may reflect higher sensitivity of flow cytometry.

3.3. GL7 expression is increased on CNS B cells after control of infectious virus

Both peripheral and CNS viral infections in mice deficient in the lymphoid organizing chemokine CXCL13 elicit B cell isotype switching and virus specific serum Ab despite impaired GC formation (Phares et al., 2016; Rainey-Barger et al., 2011). We therefore hypothesized that B cells recruited to the CNS may be locally activated to divide and differentiate even in the absence of follicle formation. Although we could not detect GL7 expression by immunohistochemistry, we examined early differentiated B cell subsets in the CNS for GL7 expression by more sensitive flow cytometry, which is more prone to detect lower levels of GL7 expression characteristic of activated, but not yet GC participating B cells (Cervenak et al., 2001; Naito et al., 2007). Surprisingly, the proportion of GL7 expressing CD19$^+$ B cells increased from ~8 to 25% between days 7 and 21 p.i. (Fig. 6A and B). Similar to CLN counterparts, GL7$^+$ cells segregated into an intermediate and high expressing phenotype (Fig. 6A). However, only a minor fraction were GL7^{hi} in the CNS (Fig. 6B). Mean fluorescent intensity (MFI) histograms of GL7 expression revealed that both IgD^{int} and IgD$^-$ B cells expressed lower GL7 within the CNS relative to those within

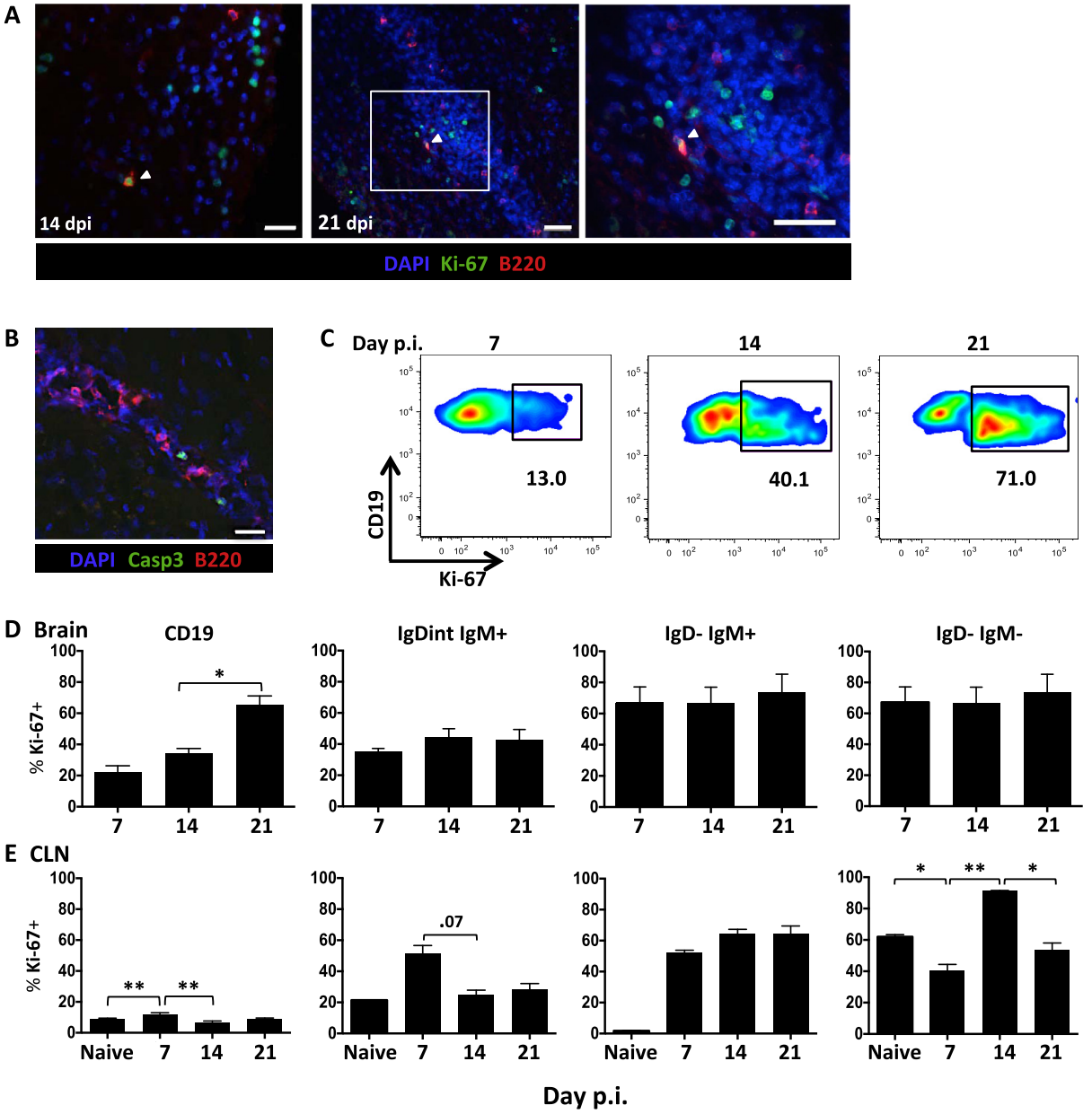

Fig. 5. B cell proliferation is sustained within the CNS in the absence of ectopic follicles. (A) B220^{+} (red) B cells within the brain were analyzed for expression of the proliferation marker Ki-67 (green) at day 14 (scale bar = 20 μm) and 21 p.i. (dpi) (scale bar = 100 μm) using confocal microscopy. Nuclei are marked by DAPI (blue). White-boxed area from day 21 p.i. shown in right image (scale bar = 100 μm). (B) Representative Z stack compilations from 2 independent experiments with 3 mice per experiment showing co-staining for B220^{+} (red), caspase-3 and DAPI (blue) at d14 p.i. (scale bar = 20 μm). (C) Representative flow cytometry density plots showing Ki-67 expression in brain derived CD45^{hi} CD19^{+} B cells at day 7, 14, and 21 p.i. Numbers below the gated population indicate the percent of Ki-67 expressing cells. Bar graphs show percentages of Ki-67^{+} cells within brain (D) and CLN (E) derived CD19^{+} B cells and within the indicated B cell subsets. Data in D-E are expressed as the mean percentage ± SEM and represent 3–4 independent experiments each comprising 3–6 pooled brains or CLN per time point. Significant differences between time points are indicated by $*$ ($p < 0.05$) and $**$ ($p < 0.01$). (For interpretation of the references to color in this figure legend, the reader is referred to the web version of this article.)

the CLN (Fig. 6C). Overall, the increasing proportion of GL7^{+} B cells within the CNS throughout infection was mainly attributed to IgD^{int} and IgD^{-} B cells with a GL7^{int} phenotype (Fig. 6D).

To further characterize the activation state of CNS B cells we analyzed expression of Fas (CD95) and CD38. GC B cells in murine lymphoid tissue express both GL7 and CD95, while CD38 is downregulated (Koncz and Hueber, 2012; Oliver et al., 1997). However, CD95 upregulation and CD38 downregulation are also markers of activation, independent of GCs (Oliver et al., 1997; Schattner et al., 1995). CLN derived B cells at day 21 p.i. indeed contained a well-defined GL7^{hi} CD95^{+} population supporting a GC phenotype (Supplementary Fig. 3A). Interestingly, CNS derived B cells exhibited a more complex expression pattern containing GL7^{+}CD95^{+}, as well as GL7^{-}CD95^{+} and GL7^{+}CD95^{-} cells. GL7^{hi} cells were all CD95^{+} (Supplementary Fig. 3A). Furthermore, all CD95^{+} populations were IgD^{-}, indicating the activated phenotype was limited to IgM^{+} or isotype-switched B cells. Lastly, while CD38 downregulation was prominent in CLN IgD^{-} B cells, it not as marked in respective CNS B cell populations (Supplementary Fig. 3B).

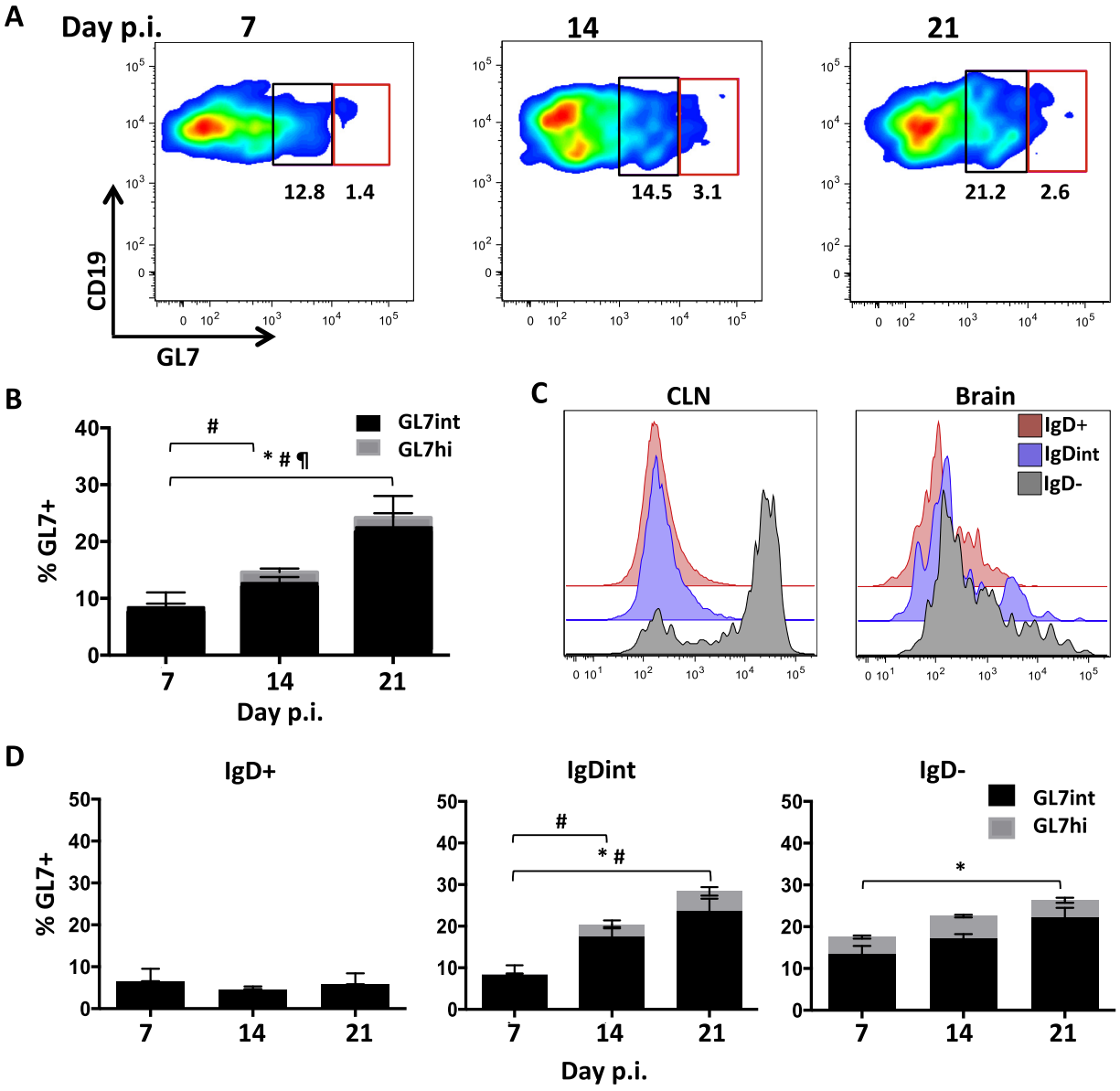

Fig. 6. GL7$^+$ B cells accumulate within the CNS during JHMV infection. Analysis of GL7 expression in brain derived B cells at day 7, 14, and 21 p.i. by flow cytometry. (A) Representative density plots showing gating strategy of GL7^{int} (black) and GL7^{hi} (red) within total CD19+ cells. Numbers in plots indicate relative percentages of GL7^{int} and GL7^{hi} populations. (B) Stacked bar graph shows increasing percentages of GL7^{int} and GL7^{hi} B cells during viral persistence. (C) Representative histogram comparing GL7 expression intensity on IgD$^+$ (red), IgD^{int} (blue), and IgD$^-$ (gray) B cell subsets within CLN and Brain at day 14 p.i. (D) Relative percentages of GL7^{int} and GL7^{hi} cells within IgD$^+$, IgD^{int}, or IgD$^-$ brain derived CD19$^+$ B cells at day 7, 14, and 21 p.i. Data in (B) and (D) are expressed as the mean percentage ± SEM and represent 3–4 independent experiments each comprising 3–6 pooled brains per time point. Significant differences between time points are indicated by $*$ ($p \leqslant 0.05$) for GL7int, # ($p \leqslant 0.05$) for GL7hi, and ¶ ($p \leqslant 0.05$) for total GL7 + cells. (For interpretation of the references to color in this figure legend, the reader is referred to the web version of this article.)

3.4. Activated and differentiated B cells express a "helped" phenotype within the CNS throughout infection

The high proportion of GL7^{int} cells in differentiated CNS B cell subsets suggested local CD4 T cell help contributes to sustained GL7 upregulation. B cell/T cell interactions are characterized by early CD40 upregulation, and subsequent surface expression of CD80 on B cells (Banchereau et al., 1994; Clatza et al., 2003; Yellin et al., 1994). CD80 signaling promotes B cell survival, proliferation, and differentiation (Clatza et al., 2003). CD40 and CD80 expression on CNS B cells was therefore analyzed by flow cytometry as a signature of CD4 T cell help. CD40 expression on CNS B cells was very modest (Fig. 7A/C) and mainly elevated on early infiltrating IgD$^-$IgM$^+$ and IgD$^-$IgM$^-$ populations at day 7 p.i. with peak expression at ~20% (Fig. 7C). By contrast, CD80 expression increased from 20% at day 7 p.i. to 50% at day 14 p.i., and was further elevated to 75% day 21 p.i. (Fig. 7B/D). While CD80 was detectable on a small population of naïve phenotype B cells (<15%; data not shown), it was most strongly upregulated on IgD^{int}IgM$^+$ cells and prominent on IgD$^-$IgM$^+$ and isotype-switched B cells at day 14 p.i. (Fig. 7D). The high proportion of CD80 expressing IgD^{int} and IgD$^-$ B cell subsets was sustained throughout day 21 p.i. Distinct from the sustained expression of activation markers within the CNS, both CD40 (data not shown) and CD80 expression on total CD19$^+$ B cells within the CLN peaked at day 7 p.i. and followed distinct kinetics on individual subsets (Fig. 7D). CD80 expression on naïve phenotype CLN B cells peaked at ~5% at day 7 (data not shown), but remained constitutive at ~30% on IgD^{int} IgM$^+$ cells

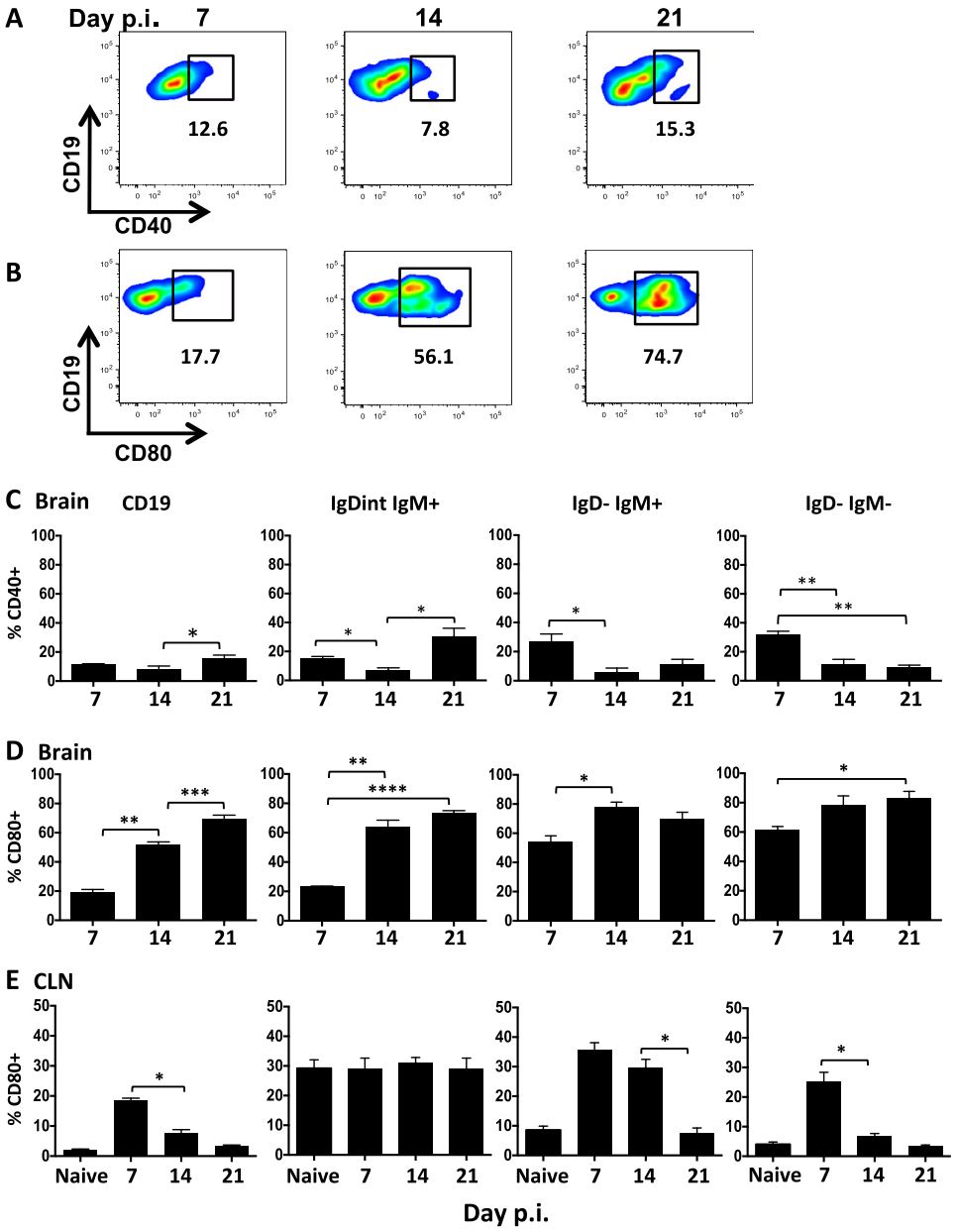

Fig. 7. Activated and differentiated B cells express markers of CD4 T cell help within the brain. Representative density plots and gating of CD40 (A) and CD80 (B) expression on brain derived CD45^{hi}CD19^{+} B cells at day 7, 14, and 21 p.i. Percentages of CD40^{+} cells (C) or CD80^{+} cells (D,E) within total CD19^{+} or the indicated B cell subsets derived from brain (C,D) or CLN (E) determined by flow cytometry. Data are expressed as the mean percentage ± SEM and represent 3–4 independent experiments each comprising 3–6 pooled brain or CLN per time point. Statistically significant differences between time points are indicated by $* p \leqslant 0.05$, $** p \leqslant 0.01$, $*** p \leqslant 0.001$ and $**** p \leqslant 0.0001$.

similar to baseline levels in naïve mice. Moreover, while CD80 was significantly upregulated on IgD^{-}IgM^{+} and isotype-switched B cells at day 7 relative to naïve mice, it was not sustained and declined to background levels by day 21 p.i. (Fig. 7E). Sustained CD80 expression within the CNS therefore supports a contribution of continued local T cell-B cell interactions in driving an activated phenotype.

The presence of highly activated B cells expressing markers of CD4 T cell help in the absence of apparent defined follicles led us to examine whether B cells co-localize with CD4 T cells. Overall CD4 T cells vastly outnumbered B cells and were distributed in both perivascular and parenchymal sites (Fig. 8A). Although many B cells and T cells localized to individual domains, we also observed occasional clusters of B and T cells in anatomical sites resembling perivascular space (Fig. 8A). Of note, in areas of B and T cell proximity, individual B cells appeared in close contact with multiple T cells (Fig. 8B). Moreover, overlapping B220 and CD3 membrane staining by confocal analysis supported direct interactions (Fig. 8C). These results suggest that establishment of JHMV persistence at day 14 p.i. is associated with ongoing B cell activation and proliferation aided by CD4 T cells independent of ectopic follicle formation.

4. Discussion

Activated, differentiated, and proliferating B cells within inflamed non-lymphoid tissue, including the CNS, have been associated with the formation of ectopic follicles (Carragher et al., 2008; Pitzalis et al., 2014; Magliozzi et al., 2007; Peters et al., 2011; Serafini et al., 2004). However, recent studies indicating that B cells populating the MS brain mature in the CLN also support

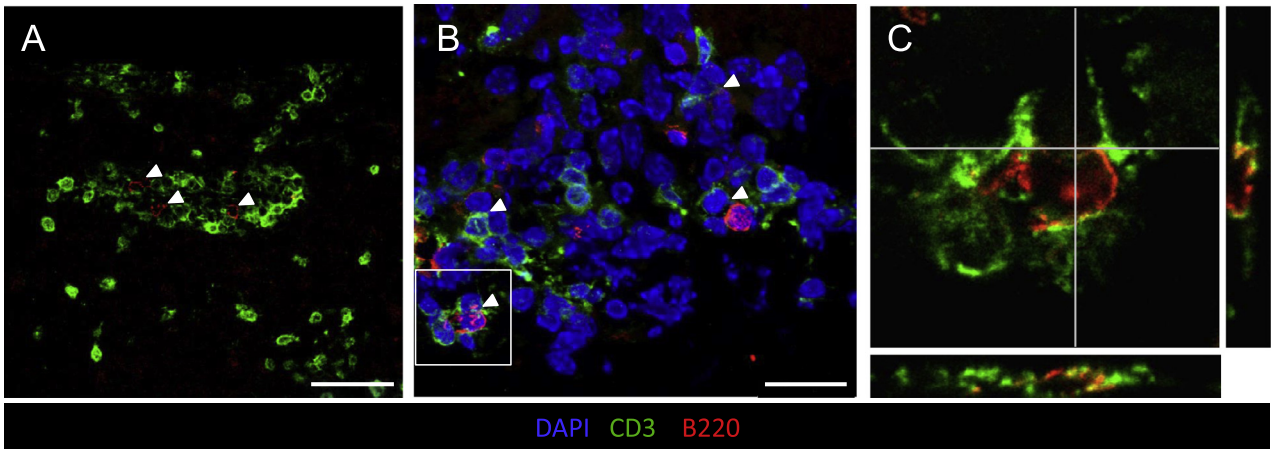

Fig. 8. B cells associate with T cells within the CNS independent of follicle formation. (A) B220$^+$ B cells (red) were co-stained with CD3$^+$ T cells (green) at day 14 p.i. B and T cell interactions were found independent of follicle structures, but frequent within perivascular and meningeal structures. Scale bar is = 50 μm. (B) Representative Z stacks of CD3 (green), B220 (red) and DAPI (blue) at day 14 p.i. reveal multiple B cell-T cell interactions (white arrows). Scale bar = 20 μm. White box indicates area selected to confirm interactions using (C) z stack projected orthogonal views of B220 and CD3. Representative images from 2 experiments with 3 mice per experiment. (For interpretation of the references to color in this figure legend, the reader is referred to the web version of this article.)

ongoing B cell trafficking between the CLN and CNS (Stern et al., 2014; Palanichamy et al., 2014). Various B cell subsets are also present during virus induced encephalomyelitis, but B cell aggregation reminiscent of follicles has not been described (Metcalf and Griffin, 2011; Metcalf et al., 2013; Rainey-Barger et al., 2011). We therefore questioned whether CNS maintenance of increasingly differentiated isotype-switched B cell subsets over time corresponds with peripheral activation and maturation, independent of CNS follicle formation during gliatropic JHMV infection.

Following JHMV infection, the apparently indiscriminate transient early increase of CLN B cells, including isotype-switched cells, coincident with increased CLN cellularity is consistent with non-specific polyclonal activation driven by innate immunity (Rothaeusler and Baumgarth, 2010). While this increase correlated with peak B cell accumulation in the brain, including early IgD$^+$ and IgD$^-$IgM$^+$ subsets, the delayed emergence of isotype-switched B cells rather coincided with formation of GC in CLN. Interestingly, the vast expansion of ASC in CLN prior to appearance of virus specific ASC, was also not associated with migration into the CNS (Marques et al., 2011). Similar to isotype-switched B cells, virus specific ASC do not start accumulating in the CNS until their peak in CLN (Marques et al., 2011; Tschen et al., 2002). These results suggest that innate activation endows migratory and CLN egress capacity to IgD$^+$ and IgD$^-$IgM$^+$ B cells. However, the delayed CNS increase in both isotype-switched B cells and ASC supports that a subsequent phase of antigen driven differentiation coincident with GC maturation imprints isotype-switched B cells and ASC to traffic to the CNS. While we cannot exclude that early activated B cells migrating to the CNS receive local signals to further differentiate, the absence of GC-like structures in the meninges and inability to detect virus specific IgG$^+$ B cells in the CNS early during infection does not favor this notion. Moreover, RNA analysis of B cell subsets did not reveal evidence of AID expression in CNS B cells (Phares et al., 2014), an enzyme expressed in GC B cells and critical for hypermutation and class switching (Crouch et al., 2007; Maul and Gearhart, 2010; Phares et al., 2014).

The signals regulating egress of distinct B cell subsets from the CLN remain to be scrutinized, but likely involve complex regulation of multiple chemokine receptors and S1P1 (Cupovic et al., 2016; Cyster, 2005; Cyster and Schwab, 2012; Okada and Cyster, 2006). Although the upregulation of CXCL13 during most neuroinflammatory insults suggested it recruits CXCR5$^+$ naïve or early activated B cells, the absence of CXCL13 did not alter early recruitment of B cells to the CNS during EAE or JHMV infection (Phares et al., 2016; Rainey-Barger et al., 2011). B cells are further guided within lymphoid organs by CCR7 ligands CCL19 and CCL21, lymphoid chemokines which are also expressed in the CNS (Lalor and Segal, 2010). Specifically, production of CCR7 ligands by CNS stromal cells which supports CCR7$^+$ CD8 T cell recruitment from the CLN to the infected CNS (Cupovic et al., 2016), provides a likely mechanism for early B cell recruitment. This is supported by expression of CCR7 transcripts in IgD$^+$ and to a lesser extent IgD$^-$ B cells in the CNS at day 7 p.i. (Phares et al., 2014), whereas CXCR5 transcripts are downregulated compared to CLN IgD$^+$ populations. Although IgD$^+$ and IgD$^-$ B cells as well as ASC in the CNS have very low levels of S1P1 relative to IgD+ cells in CLN during JHMV infection (Phares et al., 2014), the temporal contribution of S1P1 regulation on B cell egress from CLN has not been well explored.

The primary anatomical localization of early B cells, comprising mainly IgD$^+$ and /or IgM$^+$ cells, to the meninges and perivascular spaces resembled observations in MS and EAE. Interestingly, isotype-switched IgG$^+$ B cells prevailing at later times were prominent in the parenchyma, suggesting distinct guidance by migratory cues. While CCR7 ligands derived from stromal cells may restrict early activated CCR7$^+$ B cells to extraparenchymal sites, B cell migration is also guided by CXCR4 ligand CXCL12, which is constitutively expressed in the CNS. While CXCL12 presentation on the luminal side arrests lymphocyte entry into the parenchyma, its sequestration by binding to CXCR7 on activated endothelial cells, allows parenchymal lymphocyte access (Cruz-Orengo et al., 2011). Similarly complex mechanisms may underlie preferential entry of isotype-switched B cells into the parenchyma. While the mechanisms underlying parenchymal B cell infiltration remain to be resolved, they are independent of BBB integrity, as the BBB permeability is restored to naïve levels by day 14 p.i. (Phares et al., 2014). Interestingly, CD138+ ASC also mainly localize to the parenchyma, where they are dispersed in the white matter (Marques et al., 2011; Tschen et al., 2006). This process appears driven by astrocyte derived CXCL10 (Phares et al., 2013b).

Parenchymal B cell entry may further be regulated by the B cell activation state. Although the absence of CNS ectopic follicle formation driving activation during JHMV infection was supported by few or no clustered B cells expressing Ki-67, undergoing apoptosis, or expressing GL7 by histological analysis, flow cytometry demonstrated a high proportion of both Ki-67$^+$, GL7$^+$ and CD95$^+$ cells mainly in the IgD$^-$ populations. Although Ki-67 and GL7

expression intensity was lower relative to CLN derived B cells, it was sustained throughout infection, unlike transient expression in CLN counterparts. The overall paucity of $GL7^{hi}$ B cells supported the inability to detect GC B cells in the CNS by histology. The $GL7^{int}$ phenotype may be driven by ongoing local cytokine, complement, or antigen driven activation during chronic infection. Local activation was supported by a large fraction of CD95 expressing cells and sustained expression of CD80 as a marker for CD4 T cell interactions. Although CD4 T cells were overall more abundant than B cells, occasional interactions were indicated by close proximity and overlapping membrane staining. Moreover, a single CD4 T cell appeared to interact with multiple B cells, suggesting few CD4 T cells may imprint a large number of B cells. This notion is supported by detection of CD4 T cell derived IL-21 as well as ongoing CNS expression of CXCL13, CCL19 and CCL21 within the JHMV infected CNS (Phares et al., 2011, 2013a, 2014, 2016). These lymphoid chemokines may facilitate proximal localization of CD4 T cells and B cells especially at meningeal or perivascular sites, which also harbor antigen presenting cells driving CD4 T cell reactivation (Kivisakk et al., 2009; Ransohoff and Engelhardt, 2012).

While activation markers on B cells have not been assessed during Sindbis virus induced encephalitis, B cell maintenance also appears independent of follicle formation. Moreover, in a spontaneous autoimmune model of EAE, meningeal B cell infiltrates clustered and expressed activated phenotype, but did not show follicular features (Dang et al., 2015). Although the functional consequences of sustained B cell activation remain to be determined, $GL7^{+}$ B cells have higher functional activity for producing antibodies and presenting antigens. It is thus tempting to propose that virus specific $GL7^{+}$ IgM^{+} or IgG^{+} B cells may function to present persisting viral Ag within the CNS to reactivate residual T cells. In this context, it is interesting to note that stored, unprocessed antigen released from dendritic cells can be transferred to B cells potentially contributing to their activation (Le Roux et al., 2012).

The apparent absence of ectopic follicle formation during JHMV or Sindbis virus encephalomyelitis may be due to the paucity of IL-17 in these models. Th17 cells are a primary driver of ectopic follicle formation (Grogan and Ouyang, 2012; Peters et al., 2011). While Th17 cells are a pathogenic component during autoimmune mediated inflammation, they are generally poorly induced during viral infections (Martinez et al., 2012). Neurotropic MHV infections are dominated by Th1 responses with little or no contribution of Th17 cells (Kapil et al., 2009). Although CXCL13, required for follicle and GC organization, is produced in the CNS during JHMV infection, CXCL13 deficient mice still mount protective serum Ab responses despite reduced peripheral GC formation. The development of humoral immunity in CXCL13 deficient mice infected peripherally with other viruses, despite impaired follicle and GC formation, provides further evidence that B cells can differentiate independent of defined GC structures (Phares et al., 2016).

In summary, our results show highly dynamic local maintenance of activated B cells independent of follicle formation within the CNS during JHMV infection. The data support the concept that immune events in the CLN initiate B cell subset migration with additional signals in the CNS, such as CD4 T cell interactions, determining anatomical localization and ongoing activation of distinct B cell subsets at the site of inflammation.

Acknowledgments

This work was supported by US National Institutes of Health grant NS086299 and a 2015 US National Institutes of Health shared instrument award to the Lerner Resaerch Institute Imaging Core for the Leica TCS-SP5II. The funding source had no involvement in study design, writing of the manuscript, decision to submit or collection, analysis and interpretation of data. We sincerely thank Mi Widness for exceptional technical assistance and Dr. Mi-Hyun Hwang for viral CNS infection.

Appendix A. Supplementary data

Supplementary data associated with this article can be found, in the online version, at http://dx.doi.org/10.1016/j.bbi.2016.09.022.

References

Ankeny, D.P. et al., 2006. Spinal cord injury triggers systemic autoimmunity: evidence for chronic B lymphocyte activation and lupus-like autoantibody synthesis. J Neurochem. 99, 1073–1087.
Ankeny, D.P., Guan, Z., Popovich, P.G., 2009. B cells produce pathogenic antibodies and impair recovery after spinal cord injury in mice. J. Clin. Invest. 119, 2990–2999.
Avasarala, J.R., Cross, A.H., Trotter, J.L., 2001. Oligoclonal band number as a marker for prognosis in multiple sclerosis. Archit. Neurol. 58, 2044–2045.
Balogh, A. et al., 2010. A closer look into the GL7 antigen: its spatio-temporally selective differential expression and localization in lymphoid cells and organs in human. Immunol. Lett. 130, 89–96.
Banchereau, J. et al., 1994. The CD40 antigen and its ligand. Ann. Rev. Immunol. 12, 881–922.
Bankoti, J. et al., 2014. In multiple sclerosis, oligoclonal bands connect to peripheral B-cell responses. Ann. Neurol. 75, 266–276.
Bar-Or, A. et al., 2010. Abnormal B-cell cytokine responses a trigger of T-cell-mediated disease in MS? Ann. Neurol. 67, 452–461.
Bombardieri, M. et al., 2012. Inducible tertiary lymphoid structures, autoimmunity, and exocrine dysfunction in a novel model of salivary gland inflammation in C57BL/6 mice. J. Immunol. 189, 3767–3776.
Carlsen, H.S. et al., 2002. B cell attracting chemokine 1 (CXCL13) and its receptor CXCR5 are expressed in normal and aberrant gut associated lymphoid tissue. Gut. 51, 364–371.
Carragher, D.M., Rangel-Moreno, J., Randall, T.D., 2008. Ectopic lymphoid tissues and local immunity. Semin. Immunol. 20, 26–42.
Cepok, S. et al., 2005. Short-lived plasma blasts are the main B cell effector subset during the course of multiple sclerosis. Brain 128, 1667–1676.
Cervenak, L. et al., 2001. Differential expression of GL7 activation antigen on bone marrow B cell subpopulations and peripheral B cells. Immunol. Lett. 78, 89–96.
Claes, N. et al., 2015. B cells are multifunctional players in multiple sclerosis pathogenesis: insights from therapeutic interventions. Front. Immunol. 6, 642.
Clatza, A. et al., 2003. CD40-induced aggregation of MHC class II and CD80 on the cell surface leads to an early enhancement in antigen presentation. J. Immunol. 171, 6478–6487.
Corcione, A. et al., 2004. Recapitulation of B cell differentiation in the central nervous system of patients with multiple sclerosis. Proc. Natl. Acad. Sci. USA 101, 11064–11069.
Crouch, E.E. et al., 2007. Regulation of AID expression in the immune response. J. Exp. Med. 204, 1145–1156.
Cruz, M. et al., 1987. Immunoblot detection of oligoclonal anti-myelin basic protein IgG antibodies in cerebrospinal fluid in multiple sclerosis. Neurology 37, 1515–1519.
Cruz-Orengo, L. et al., 2011. CXCR7 influences leukocyte entry into the CNS parenchyma by controlling abluminal CXCL12 abundance during autoimmunity. J. Exp. Med. 208, 327–339.
Cupovic, J. et al., 2016. Central nervous system stromal cells control local CD8(+) T cell responses during virus-induced neuroinflammation. Immunity 44, 622–633.
Cyster, J.G., 2005. Chemokines, sphingosine-1-phosphate, and cell migration in secondary lymphoid organs. Ann. Rev. Immunol. 23, 127–159.
Cyster, J.G., Schwab, S.R., 2012. Sphingosine-1-phosphate and lymphocyte egress from lymphoid organs. Ann. Rev. Immunol. 30, 69–94.
Dang, A.K. et al., 2015. Meningeal infiltration of the spinal cord by non-classically activated B cells is associated with chronic disease course in a spontaneous B cell-dependent model of CNS autoimmune disease. Front. Immunol. 6, 470.
Fleming, J.O. et al., 1986. Pathogenicity of antigenic variants of murine coronavirus JHM selected with monoclonal antibodies. J. Virol. 58, 869–875.
Grogan, J.L., Ouyang, W., 2012. A role for Th17 cells in the regulation of tertiary lymphoid follicles. Eur. J. Immunol. 42, 2255–2262.
Hauser, S.L. et al., 2008. B-cell depletion with rituximab in relapsing-remitting multiple sclerosis. N. Engl. J. Med. 358, 676–688.
Hawkins, E.D. et al., 2013. Quantal and graded stimulation of B lymphocytes as alternative strategies for regulating adaptive immune responses. Nat. Commun. 4, 2406.
Junt, T. et al., 2005. CXCR5-dependent seeding of follicular niches by B and Th cells augments antiviral B cell responses. J. Immunol. 175, 7109–7116.
Kapil, P. et al., 2009. Interleukin-12 (IL-12), but not IL-23, deficiency ameliorates viral encephalitis without affecting viral control. J. Virol. 83, 5978–5986.
Kappos, L. et al., 2014. Atacicept in multiple sclerosis (ATAMS): a randomised, placebo-controlled, double-blind, phase 2 trial. Lancet Neurol. 13, 353–363.
Kivisakk, P. et al., 2009. Localizing central nervous system immune surveillance: meningeal antigen-presenting cells activate T cells during experimental autoimmune encephalomyelitis. Ann. Neurol. 65, 457–469.

Koncz, G., Hueber, A.O., 2012. The Fas/CD95 receptor regulates the death of autoreactive B cells and the selection of antigen-specific B cells. Front. Immunol. 3, 207.
Kowarik, M.C. et al., 2012. CXCL13 is the major determinant for B cell recruitment to the CSF during neuroinflammation. J. Neuroinflammation 9, 93.
Krumbholz, M. et al., 2006. Chemokines in multiple sclerosis: CXCL12 and CXCL13 up-regulation is differentially linked to CNS immune cell recruitment. Brain 129, 200–211.
Lalor, S.J., Segal, B.M., 2010. Lymphoid chemokines in the CNS. J. Neuroimmunol. 224, 56–61.
Laman, J.D., Weller, R.O., 2013. Drainage of cells and soluble antigen from the CNS to regional lymph nodes. J. Neuroimmune Pharmacol. 8, 840–856.
Le Roux, D. et al., 2012. Antigen stored in dendritic cells after macropinocytosis is released unprocessed from late endosomes to target B cells. Blood 119, 95–105.
Lehmann-Horn, K. et al., 2011. Anti-CD20 B-cell depletion enhances monocyte reactivity in neuroimmunological disorders. J. Neuroinflammation 8, 146.
Lin, M.T. et al., 1999. Antibody prevents virus reactivation within the central nervous system. J. Immunol. 162, 7358–7368.
Lino, A.C. et al., 2016. Cytokine-producing B cells: a translational view on their roles in human and mouse autoimmune diseases. Immunol. Rev. 269, 130–144.
Lisak, R.P. et al., 2012. Secretory products of multiple sclerosis B cells are cytotoxic to oligodendroglia in vitro. J. Neuroimmunol. 246, 85–95.
Magliozzi, R. et al., 2004. Intracerebral expression of CXCL13 and BAFF is accompanied by formation of lymphoid follicle-like structures in the meninges of mice with relapsing experimental autoimmune encephalomyelitis. J. Neuroimmunol. 148, 11–23.
Magliozzi, R. et al., 2007. Meningeal B-cell follicles in secondary progressive multiple sclerosis associate with early onset of disease and severe cortical pathology. Brain 130, 1089–1104.
Malmestrom, C. et al., 2006. IL-6 and CCL2 levels in CSF are associated with the clinical course of MS: implications for their possible immunopathogenic roles. J. Neuroimmunol. 175, 176–182.
Marques, C.P. et al., 2011. CXCR3-dependent plasma blast migration to the central nervous system during viral encephalomyelitis. J. Virol. 85, 6136–6147.
Martinez, N.E. et al., 2012. Regulatory T cells and Th17 cells in viral infections: implications for multiple sclerosis and myocarditis. Future Virol. 7, 593–608.
Maseda, D. et al., 2012. Regulatory B10 cells differentiate into antibody-secreting cells after transient IL-10 production in vivo. J. Immunol. 188, 1036–1048.
Matsushita, T. et al., 2008. Regulatory B cells inhibit EAE initiation in mice while other B cells promote disease progression. J. Clin. Invest. 118, 3420–3430.
Matsushita, T. et al., 2010. Regulatory B cells (B10 cells) and regulatory T cells have independent roles in controlling experimental autoimmune encephalomyelitis initiation and late-phase immunopathogenesis. J. Immunol. 185, 2240–2252.
Maul, R.W., Gearhart, P.J., 2010. AID and somatic hypermutation. Adv. Immunol. 105, 159–191.
Metcalf, T.U., Griffin, D.E., 2011. Alphavirus-induced encephalomyelitis: antibody-secreting cells and viral clearance from the nervous system. J. Virol. 85, 11490–11501.
Metcalf, T.U. et al., 2013. Recruitment and retention of B cells in the central nervous system in response to alphavirus encephalomyelitis. J. Virol. 87, 2420–2429.
Michel, L. et al., 2015. B cells in the multiple sclerosis central nervous system: trafficking and contribution to CNS-compartmentalized inflammation. Front. Immunol. 6, 636.
Naito, Y. et al., 2007. Germinal center marker GL7 probes activation-dependent repression of N-glycolylneuraminic acid, a sialic acid species involved in the negative modulation of B-cell activation. Mol. Cell Biol. 27, 3008–3022.
Niino, M. et al., 2009. Memory and naive B-cell subsets in patients with multiple sclerosis. Neurosci. Lett. 464, 74–78.
Okada, T., Cyster, J.G., 2006. B cell migration and interactions in the early phase of antibody responses. Curr. Opin. Immunol. 18, 278–285.
Oliver, A.M., Martin, F., Kearney, J.F., 1997. Mouse CD38 is down-regulated on germinal center B cells and mature plasma cells. J. Immunol. 158, 1108–1115.
Owens, G.P. et al., 2011. Viruses and multiple sclerosis. Neuroscientist 17, 659–676.
Palanichamy, A. et al., 2014. Immunoglobulin class-switched B cells form an active immune axis between CNS and periphery in multiple sclerosis. Sci. Transl. Med. 6, 248ra106.
Parker Harp, C.R. et al., 2015. B cell antigen presentation is sufficient to drive neuroinflammation in an animal model of multiple sclerosis. J. Immunol. 194, 5077–5084.
Peters, A. et al., 2011. Th17 cells induce ectopic lymphoid follicles in central nervous system tissue inflammation. Immunity 35, 986–996.
Phares, T.W. et al., 2011. Factors supporting intrathecal humoral responses following viral encephalomyelitis. J. Virol. 85, 2589–2598.
Phares, T.W. et al., 2013a. IL-21 optimizes T cell and humoral responses in the central nervous system during viral encephalitis. J. Neuroimmunol. 263, 43–54.
Phares, T.W. et al., 2013b. Astrocyte-derived CXCL10 drives accumulation of antibody-secreting cells in the central nervous system during viral encephalomyelitis. J. Virol. 87, 3382–3392.
Phares, T.W. et al., 2014. Progression from IgD^+ IgM^+ to isotype-switched B cells is site specific during coronavirus-induced encephalomyelitis. J. Virol. 88, 8853–8867.
Phares, T.W. et al., 2016. CXCL13 promotes isotype-switched B cell accumulation to the central nervous system during viral encephalomyelitis. Brain Behav. Immunol.
Pierson, E.R., Stromnes, I.M., Goverman, J.M., 2014. B cells promote induction of experimental autoimmune encephalomyelitis by facilitating reactivation of T cells in the central nervous system. J Immunol. 192, 929–939.
Pikor, N.B. et al., 2015. Meningeal Tertiary Lymphoid Tissues and Multiple Sclerosis: A Gathering Place for Diverse Types of Immune Cells during CNS Autoimmunity. Front. Immunol. 6, 657.
Pitzalis, C. et al., 2014. Ectopic lymphoid-like structures in infection, cancer and autoimmunity. Nat. Rev. Immunol. 14, 447–462.
Rainey-Barger, E.K. et al., 2011. The lymphoid chemokine, CXCL13, is dispensable for the initial recruitment of B cells to the acutely inflamed central nervous system. Brain Behav. Immunol. 25, 922–931.
Ransohoff, R.M., Engelhardt, B., 2012. The anatomical and cellular basis of immune surveillance in the central nervous system. Nat. Rev. Immunol. 12, 623–635.
Rothaeusler, K., Baumgarth, N., 2010. B-cell fate decisions following influenza virus infection. Eur. J. Immunol. 40, 366–377.
Schattner, E.J. et al., 1995. CD40 ligation induces Apo-1/Fas expression on human B lymphocytes and facilitates apoptosis through the Apo-1/Fas pathway. J. Exp. Med. 182, 1557–1565.
Serafini, B. et al., 2004. Detection of ectopic B-cell follicles with germinal centers in the meninges of patients with secondary progressive multiple sclerosis. Brain Pathol. 14, 164–174.
Shen, P. et al., 2014. IL-35-producing B cells are critical regulators of immunity during autoimmune and infectious diseases. Nature 507, 366–370.
Shi, K. et al., 2001. Lymphoid chemokine B cell-attracting chemokine-1 (CXCL13) is expressed in germinal center of ectopic lymphoid follicles within the synovium of chronic arthritis patients. J. Immunol. 166, 650–655.
Stern, J.N. et al., 2014. B cells populating the multiple sclerosis brain mature in the draining cervical lymph nodes. Sci. Transl. Med. 6, 248ra107.
Stohlman, S.A. et al., 1995. Mouse hepatitis virus-specific cytotoxic T lymphocytes protect from lethal infection without eliminating virus from the central nervous system. J. Virol. 69, 684–694.
Tedder, T.F., 2015. B10 cells: a functionally defined regulatory B cell subset. J. Immunol. 194, 1395–1401.
Tschen, S.I. et al., 2002. Recruitment kinetics and composition of antibody-secreting cells within the central nervous system following viral encephalomyelitis. J. Immunol. 168, 2922–2929.
Tschen, S.I. et al., 2006. CNS viral infection diverts homing of antibody-secreting cells from lymphoid organs to the CNS. Eur. J. Immunol. 36, 603–612.
Warren, K.G., Catz, I., 1994. Relative frequency of autoantibodies to myelin basic protein and proteolipid protein in optic neuritis and multiple sclerosis cerebrospinal fluid. J. Neurol. Sci. 121, 66–73.
Weber, M.S. et al., 2010. B-cell activation influences T-cell polarization and outcome of anti-CD20 B-cell depletion in central nervous system autoimmunity. Ann. Neurol. 68, 369–383.
Weyand, C.M., Goronzy, J.J., 2003. Ectopic germinal center formation in rheumatoid synovitis. Ann. N.Y. Acad. Sci. 987, 140–149.
Xiao, S. et al., 2015. Tim-1 is essential for induction and maintenance of IL-10 in regulatory B cells and their regulation of tissue inflammation. J. Immunol. 194, 1602–1608.
Yellin, M.J. et al., 1994. T lymphocyte T cell-B cell-activating molecule/CD40-L molecules induce normal B cells or chronic lymphocytic leukemia B cells to express CD80 (B7/BB-1) and enhance their costimulatory activity. J. Immunol. 153, 666–674.